Fast CO2 uptake by intense weathering of volcanic islands during interglacial stages

Francisco Hevia-Cruz, Anthony Hildenbrand, Nathan D Sheldon, François Chabaux, Fernando O Marques, Julie Carlut

Geochimica et Cosmochimica Acta 401 (2025) 62–76

Contents lists available at ScienceDirect

Geochimica et Cosmochimica Acta

journal homepage: www.elsevier.com/locate/gca

Fast CO_2 uptake by intense weathering of volcanic islands during interglacial stages

Francisco Hevia-Cruz [a,b,c,*], Anthony Hildenbrand [a], Nathan D. Sheldon [d], François Chabaux [e], Fernando O. Marques [1], Julie Carlut [f]

[a] Université Paris-Saclay, CNRS, GEOPS, 91405 Orsay, France
[b] Laboratoire de Sciences du Climat et de l'Environnement, CNRS, IPSL and Sorbonne Université, 91191 Gif-sur-Yvette, France
[c] Departmento de Ciencias de la Tierra, Facultad de Ciencias Químicas, Universidad de Concepción, Chile
[d] Department of Earth and Environmental Sciences, University of Michigan, USA
[e] Université de Strasbourg, CNRS, ITES, 67084 Strasbourg, France
[f] Université Paris Cité, CNRS, Institut de Physique du Globe de Paris, 75005 Paris, France

ARTICLE INFO

Associate Editor: Cécile Gautheron

Keywords:
Pulsed soil formation
Paleosol geochemistry
Azores volcanic archipelago
Enhanced weathering
atmospheric CO_2 uptake

ABSTRACT

The weathering of basaltic rocks, especially on volcanic islands, plays a crucial role in global carbon cycling. Intense precipitation and warm atmospheric conditions accelerate weathering processes in these environments. While most estimates of weathering rates derive from river chemistry, soils and paleosols remain underexplored. In this study, we investigated the geochemistry of paleosols developed from volcanic rocks in the Azores Archipelago over the past 1 Myr. Precise geochronology of volcanic units bracketing paleosols indicates high soil formation rates (3–180 mm kyr^{-1}), similar to modern soil formation rates in tropical volcanic islands. Geochronological evidence suggests a logarithmic decrease of soil formation rates over time, with high initial values reaching near zero in less than 35 kyr. This might be attributed to a combination of cation depletion and precipitation of stable minerals. Paleosols have generally developed faster on pyroclastic deposits than on lava flows. However, those formed on lava flows required less vertical development to sustain high cation exports due to their higher density. Based on the geochemistry of paleosols and their parental materials, we estimated cation exports (0–2600 t km^{-2} yr^{-1}) and associated CO_2 uptake (0–35 × 10^6 Mol km^{-2} yr^{-1}). These estimates generally exceed previous estimates based on the geochemistry of modern rivers in the Eastern Azores, by a factor of up to tenfold. Our data highlight the transient character of weathering processes and the criticality of precise geochronological control to constrain past weathering and soil formation rates. They further imply that atmospheric CO_2 may have experienced short episodes of intense consumption during interglacial stages, possibly contributing to subsequent cooling events over the past 1 Myr.

1. Introduction

The connection between the weathering of silicate rocks and CO_2 was first surmised by Ébelmen (1845). Subsequent work demonstrated that this process is the most significant long-term sink for atmospheric CO_2 and that weathering has modulated the global climate on long time scales throughout Earth's history (Berner et al., 1983; Gaillardet et al., 1999; Berner and Kothavala, 2001; Dessert et al., 2003; Jagoutz et al., 2016; Johansson et al., 2018). It has been proposed that a major fraction of this CO_2 uptake comes from the weathering of volcanic islands as a result of their fast dissolution kinetics, controlled by factors such as their unstable geochemistry, volcanic deposit texture, high precipitation regimes, high relief, and physical erosion (Dessert et al., 2003; Rad et al., 2007; Gaillardet et al., 2011a, 2011b; Schopka and Derry, 2012; Booth et al., 2022; Hevia-Cruz et al., 2024a). Several studies in volcanic contexts have shown that the weathering rates decrease after fresh rocks are exposed to atmospheric conditions due to elemental depletion and clay formation, with clay minerals exhibiting greater stability than mafic minerals or volcanic glass (e.g., Rad et al., 2011, 2013; Sowards et al., 2018; Börker et al., 2019; Chadwick et al., 2022). Nevertheless, the actual dynamics of weathering and the typical time lag after which rates of soil formation significantly decrease remain poorly constrained.

* Corresponding authors.
E-mail addresses: francisco.hevia-cruz@universite-paris-saclay.fr, fheviac@ug.uchile.cl (F. Hevia-Cruz).
[1] Retired, no affiliation.

https://doi.org/10.1016/j.gca.2025.05.035
Received 25 June 2024; Accepted 23 May 2025
Available online 4 June 2025

Most of the studies that estimate weathering rates and CO_2 uptake by volcanic regions are based on current river geochemistry (e.g., Gaillardet et al., 1999; Dessert et al., 2003, 2015; Rad et al., 2007; Schopka and Derry, 2012), but soils and paleosols (PSs), as the remaining product of parental rocks weathering, are promising yet relatively under-explored means for investigating such processes. The Azores Archipelago represents a unique site to study past weathering rates and processes, and to estimate associated atmospheric CO_2 uptake in volcanic islands. This group of nine volcanic islands in the Central North Atlantic (Fig. 1) sits at a critical position for understanding globally important climatic drivers such as the Azores High and the Azores Current (e.g., Martin-Garcia, 2019; Cresswell-Clay et al., 2022; Frazão et al., 2022). Furthermore, it has been shown recently that PSs in the Azores retain vital information on past atmospheric conditions and their spatial and temporal variations over the late Quaternary, allowing quantitative reconstructions of mean annual temperature and precipitation through chemical proxies (Hevia-Cruz et al., 2024a, 2024b). The stratigraphy of each island includes numerous PSs intercalated between volcanic units (Fig. 2), whose geochemistry can be used to study the weathering and diagenetic processes that produced them. Equally important, the PSs are

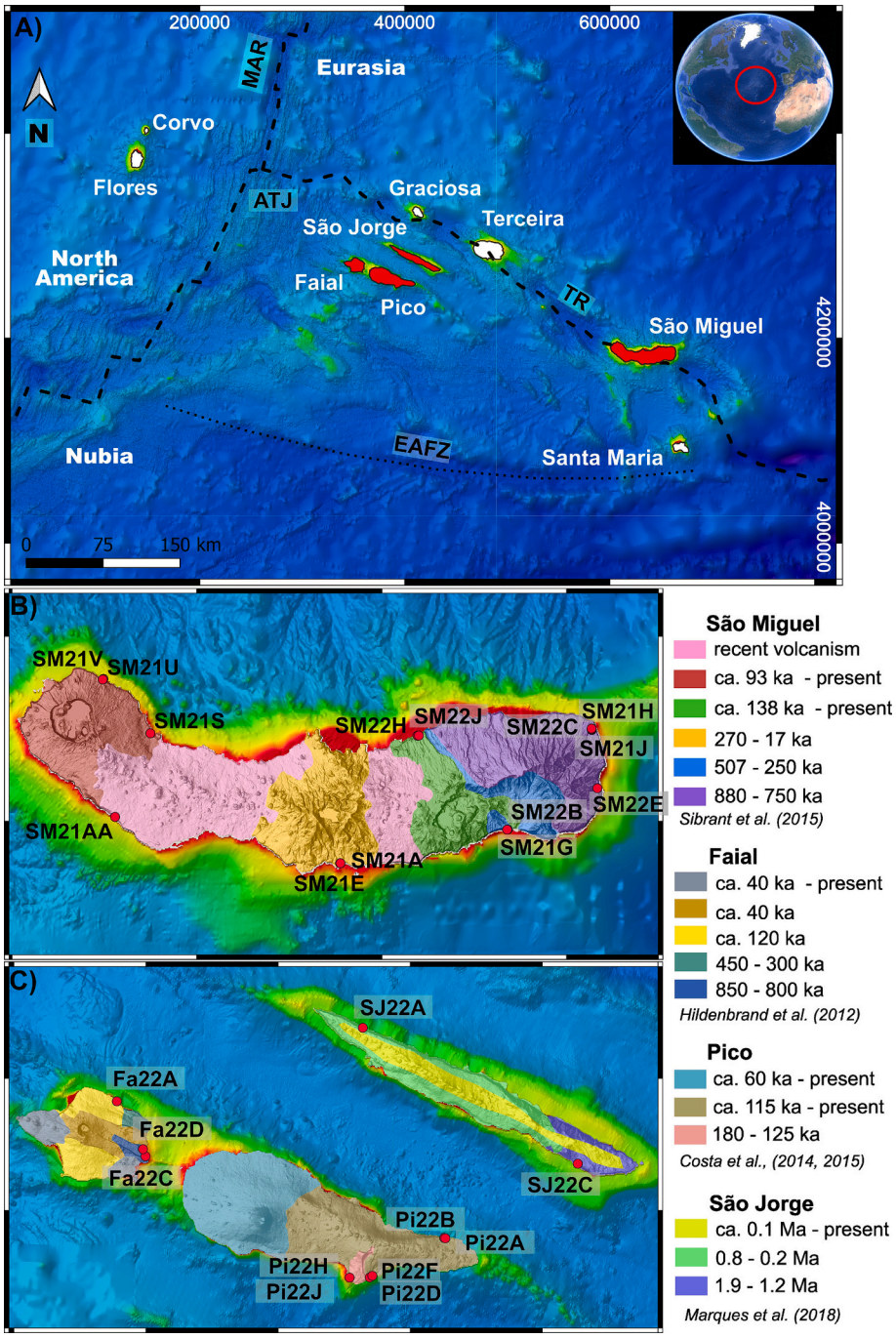

Fig. 1. Azores Archipelago and distribution of the studied paleosol (PS) profiles. A) Location and general context of the Azores. In red are highlighted the islands considered in this work (Pico, Faial, São Jorge, and São Miguel). MAR: Mid Atlantic Ridge; ATJ: Azores Triple Junction; TR: Terceira Rift; EAFZ: East Azores Fracture Zone. B) shows São Miguel Island (SM) and its age distribution (background map) after Sibrant et al. (2015), and C) shows Pico (Pi), Faial (Fa), and São Jorge (SJ) Islands and their age distributions (background maps) after Costa et al. (2014, 2015), Hildenbrand et al. (2012), and Marques et al. (2018), respectively. The red circles in B) and C) indicate the location of the PS profiles considered in this study.

bracketed by precisely dated volcanic units making it possible to constrain the time and rate of pedogenesis over the past 1 Myr (e.g., Hildenbrand et al., 2008, 2012, 2014; Costa et al., 2015; Sibrant et al., 2015; Marques et al., 2018).

This study examines the geochemistry of selected paleosol profiles with good geochronological constraints of volcanic units "bracketing" (under and overlying) them, to elucidate the weathering and soil formation rates over the past 1 Myr, and we further explore possible implications for CO_2 cycling during major climatic transitions.

2. Methods

2.1. Field and sampling strategy

Two field campaigns were carried out in 2021 and 2022 in the Central Azores islands (Pico, Faial, and São Jorge) and in São Miguel in the Eastern Azores (Fig. 1). These islands were chosen based on the high number of PSs previously recognized in the field, the good geochronological database already available, and relatively easy access to PS outcrops. The PSs were classified into three types based on the parental material on which they were formed, as described by Hevia-Cruz et al. (2024a): type I are PSs developed on the brecciated upper part of basaltic lava flows; type II are PSs developed on basic to intermediate pyroclastic deposits; and type III are PSs developed on trachytic pyroclastic deposits. Depending on the vertical variations observed in the field (color, mineralogy, texture, reaction to 10 % diluted HCl), between two and thirteen samples were collected for each PS profile, including at least one sample of each horizon comprising the fresh parental rocks. The volcanic units "bracketing" each PS profile were sampled for dating (Fig. 2). In this work, we did not perform new analyses, but the full geochronological and geochemical data can be found in the Mendeley Data repository by Hevia-Cruz et al. (2023), and their detailed analysis in Hevia-Cruz et al. (2024a, 2024b). Supplementary Table ST1 gathers the full raw data used in the present study, including the physical characterization of PSs, their geochemistry, and the geochronological data of the volcanic units bracketing them.

The PS samples were dried and grounded to powder. Major elements were analyzed by ICP-OES at SARM Laboratory after alkaline fusion with metaborate lithium ($LiBO_2$), and trace elements by HR-ICP-MS at GEOPS Laboratory after acid digestion, both in France. Uncertainties for major elements are included in the Mendeley Data repository by Hevia-Cruz et al. (2023), and trace elements measured on standard samples (BCR-2, BHVO-2, BXN, JSd-1, SL-1) were within certified expected ranges (Hevia-Cruz et al., 2024a). Fresh lava flows were dated by the unspiked K-Ar Casignol–Gillot technique (Gillot and Cornette, 1986; Gillot et al., 2006), and single-grain alkali feldspar from trachytic pyroclastic deposits were dated by $^{40}Ar/^{39}Ar$, in GEOPS and LSCE laboratories, respectively. Both techniques have been extensively used in the context of volcanic islands, including the Azores Archipelago (e.g., Hildenbrand et al., 2008, 2012, 2014, 2018, 2024; Costa et al., 2014, 2015; Sibrant et al., 2015; Marques et al., 2018; Hevia-Cruz et al., 2023, 2024a, 2024b). Typical age uncertainties of a few kyr are obtained for volcanic units younger than 1 Ma (Fig. 2). Full details including analytical procedure, age calibration and uncertainties (1σ), are given in Hevia-Cruz et al. (2024a, 2024b).

The age of PSs and the duration of weathering are determined from the precise ages obtained by either K-Ar on groundmass separates or single-grain $^{40}Ar/^{39}Ar$ analyses on alkali feldspars from volcanic units bracketing the various PSs (Hevia-Cruz et al., 2023, 2024a, 2024b). These precise ages constrain maximum and minimum PS ages. This can be seen in Fig. 2, where the difference between both lava flows mean ages is just 6 kyr (without errors), and the PS maximum formation time (including errors) is 20 kyr.

2.2. Mass transfer function

Mass transfer fluxes ($\tau_{j,w}$) were calculated following Brimhall and Dietrich (1987). For the mobile element "j" in a weathered sample "w" relative to an immobile element "i" in an unweathered parental rock "p", it is calculated as:

$$\tau_{j,w} = \frac{C_{j,w}C_{i,p}}{C_{j,p}C_{i,w}} - 1 \quad (1)$$

with $C_{j,p}$ the concentration of the mobile element "j" in "p", $C_{j,w}$ the concentration of the same element in "w", $C_{i,p}$ the concentration of "i" in "p", and $C_{i,w}$ the concentration of "i" in "w". Thus, $\tau_{j,w}$ is the elemental loss of "j" in "w" or the mass fraction of element "j" added to the system during weathering relative to the same element in the unweathered parental material. Positive $\tau_{j,w}$ indicate mass gain, whereas negative $\tau_{j,w}$ indicate mass loss. The potential diagenetic addition of alkali elements was evaluated after Sheldon (2003, 2006), by contrasting the K and Rb variations along PS profiles. We used Ti as the immobile element for our

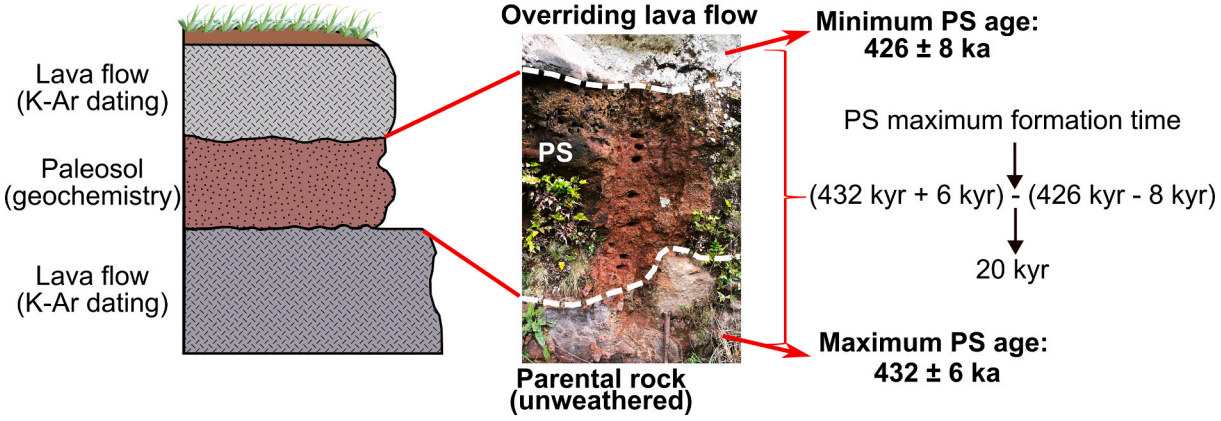

Fig. 2. Field photography illustrating our sampling strategy. Each paleosol profile was sampled vertically at different depths, depending on the characteristics observed in the field. The volcanic units "bracketing" each paleosol were sampled for geochronological purposes. The volcanic unit at the base gives the maximum paleosol age (older limit), and the volcanic unit on top gives the minimum paleosol age (younger limit). The paleosol maximum formation time corresponds to the difference between the maximum paleosol age plus its uncertainty and the minimum paleosol age minus its uncertainty.

mass transfer function calculations because, in volcanic soils, Ti is typically hosted in minerals that are highly resistant to weathering due to their stable crystal structures (Kurtz et al., 2001).

2.3. Soil formation rate estimates

To estimate the soil formation rates of the PSs "bracketed" by volcanic units, we divided each PS thickness (not including the basal unweathered parent material) by their maximum formation time. As illustrated in Fig. 2, our estimation of maximum soil formation time includes the error of both volcanic units framing ("bracketing") the PSs, in addition to the age difference between the volcanic unit setting the older age limit (lower volcanic unit) and the one setting the younger limit (upper volcanic unit sealing the profile). For PSs with variable thicknesses due to the nature of their contacts, we used a representative value between the minimum and the maximum thickness observed in the outcrop. For instance, the PS shown in Fig. 2 has a wavy contact, which makes the PS thickness variable. In the case of composite PSs (profile SM21AA) and for more than one PS constrained between two ages (profiles SM21U and SM21V) we summed the PSs' thicknesses, without considering the thickness of the intermediate parental material (i.e., we did not consider the thicknesses of the horizons SM21U5 and SM21AA6 in the total thickness of the PS; Supplementary Table ST1).

2.4. Elemental flux estimates

Elemental fluxes associated with weathering were calculated from elemental losses (expressed as Tau values) along individual profiles with respect to the fresh parental rock, the PS thicknesses, their formation duration, and the density and composition of the parental rock.

A weighted mean $\tau_{j,w}$ value was determined for each PS (assuming Ti as an immobile element), weighting each horizon's $\tau_{j,wi}$ by their thickness as $\tau_{j,w} = \sum_{i=1}^{n} \tau_{j,wi} * \frac{h_i}{h}$ where $\tau_{j,wi}$ is the mass transfer function of the horizon i, h_i the thickness of the horizon i, and h the thickness of the full PS. We used a weighted mean value because it provides an integrated elemental loss over depth, which can also be used for horizons not chemically analyzed. Using a simple mean value for every horizon or depth with measured geochemistry would be misleading, because thicker horizons would be underrepresented, and thin horizons would be overrepresented. However, for PSs where some horizons were not analyzed, we assigned them the mean $\tau_{j,w}$ value. For instance, the composite PS profile (stacked PSs where the lower horizons of the upper PS overlap the upper horizons of the lower PS; Tabor and Myers, 2015) SM21AA is made up of four single PSs, of which only two were analyzed. Consequently, the mean $\tau_{j,w}$ of the analyzed PSs was assigned to the non-analyzed PSs. Those particular cases are indicated with * in Tables 1 and 2 (and in the Supplementary Table ST2). Ca, Mg, Na, and K were considered for cation gain/loss estimates, as these four cations typically reflect the overwhelming majority of chemical weathering (e.g., Gallagher and Sheldon, 2013) except under unusually acidic weathering conditions as in some wetlands (Dzombak and Sheldon, 2020). Thus, while the calculated total flux of cations can be considered a minimum value (i.e., some CO_2 may have been consumed by trace element phases), reactions involving Ca, Mg, Na, and K should represent >90 % of the total weathering. Profiles identified as polygenetic or with diagenetic overprinting by Hevia-Cruz et al. (2024a, 2024b) were not considered for the elemental flux estimates (SM21E, SM22B, Pi22B, and Pi22H), and, consequently, they are not included in Figs. 3–6.

The mean $\tau_{j,w}$ was then multiplied by the density of the parental rock (ρ), its thickness (h), and the concentration of each element in the parental rock (C), and divided by the maximum soil-formation time (Δt; *Elemental flux* $= (\tau_{j,w} * \rho * h * C)/\Delta t$), which gave an elemental flux estimate in [g cm^{-2} kyr^{-1}], which was then converted to [t km^{-2} kyr^{-1}]. For this, we assumed an isotropic parental material and a homogeneous horizontal elemental distribution. This was then divided by each molecular weight to obtain the elemental flux in [10^6 Mol km^{-2} yr^{-1}]. We multiplied everything by −1 so that positive values are elemental losses (cations leaving the system), and negative values represent element incorporation into the system. As we did not measure the density of the fresh parental materials, we used intentionally low values compared to typical densities for the type of rocks studied here to avoid overestimating elemental fluxes: 2.5 [g cm^{-3}] for massive lava flows, 2.0 [g cm^{-3}] for fractured lava flows and basaltic tephra, and 1.0 [g cm^{-3}] for compact trachytic deposits with scarce pumice (Supplementary Table ST1; Rosi et al, 1999; Moore, 2001; Sheldon and Retallack, 2001; Polacci et al., 2003; Carmichael, 2017). The full calculations are included in Supplementary Table ST2.

3. Results

The different classifications of PSs, their thicknesses, and formation times are shown in Table 1, and the full descriptions of each PS profile and horizon can be found in Supplementary Table ST1 and in the data repository of Hevia-Cruz et al. (2023). Most PSs are classified as type I (n = 12) or as type II (n = 9), including two composite PSs, and just a few as type III (n = 3). Their thicknesses range between 18 and 550 cm (mean of 73 cm), and their maximum formation times are between 1 and 70 kyr (mean of 28 kyr; including full uncertainties; Table 1).

3.1. Soil production

Our vertical soil formation rates (soil production) estimates range between 3 [mm kyr^{-1}] and 180 [mm kyr^{-1}], with a mean of 34 [mm kyr^{-1}] (Table 1). These estimates do not consider the loss to erosion or changes in PS volume due to post-burial compaction and dilation, resulting in conservative to underestimated soil formation rates.

Those values are similar to soil formation rates observed for regions under tropical climates that are warmer and more humid than the Azores. For instance, Dosseto et al. (2022) estimated rates of 2 to 200 [mm kyr^{-1}] for soils developed on basaltic rocks at La Réunion Island. Other studies of soils formed upon intrusive rocks (Granite-granodiorite) and shale at Cameroon, Burkina Faso, Brazil, Australia, France, and the US, obtained formation rates between 20 and 70 [mm kyr^{-1}], closer to the mean value of our estimates (Boulad et al., 1977; Mathieu et al., 1995; Dequincey et al., 2002; Dosseto et al., 2008; Ma et al., 2010, 2013; Chabaux et al., 2013; Suresh et al., 2013; Ackerer et al., 2016).

3.2. Elemental fluxes

The mass transfer functions ($\tau_{j,w}$) of major elements were computed using equation (1) for the samples of the Central Azores, and those from São Miguel were previously calculated and published by Hevia-Cruz et al. (2024a), all of which are included in Fig. 3 and the Supplementary Table ST2. Values of mass transfer functions show significant variations (between −0.99 and over 9), much greater than the analytical uncertainties. Chemical variations down PS profiles generally show Ca and Mg losses, and Al, Mn and Fe tend to accumulate relative to the parental material, while the behavior of Si, Na and K varies among profiles.

Our cation export estimates (Table 2) range between −181.5 [t km^{-2} yr^{-1}] (mass addition) and 2640 [t km^{-2} yr^{-1}] (mass loss), equivalent to

Table 1
Soil formation rates, estimated from paleosol thicknesses and maximum formation time.

Profile	Paleosol type	Paleosol thickness [cm]	Maximum soil-formation time [kyr]	Minimum vertical soil formation rate [mm kyr^{-1}]
SM21H*	I	25	23	11
SM22C	I	23	34	7
SM21J*	I	29	21	14
SM22E	I	63	23	27
*SM22H**	*I*	*30*	*6*	*50*
Pi22D	I	20	33	6
Pi22F	I	43	22	20
Pi22J	I	87	29	30
Fa22A	I	60	31	19
Fa22C	I	53	26	20
FA22D	I	550	59	93
SJ22C	I	45	44	10
SM22B	II	26	3	87
SM21G*	II	27	11.8	23
SM22J	II	26	17	15
SM21U & SM21V**	II	110	70	16
SM21AA**	II	220	67	33
Pi22A*	II	85	25	34
*Pi22B**	*II*	*52*	*17*	*31*
*Pi22H***	*II*	*73*	*36*	*20*
SJ22A	II	18	1	180
SM21A	III	36	16.5	22
SM21E	*III*	*18*	*57.5*	*3*
SM21S*	III	34	9.5	36

São Miguel (SM) age data from Hevia-Cruz et al. (2024a).
Pico (Pi), Faial (Fa), and São Jorge (SJ) age data from Hevia-Cruz et al. (2024b).
(*) PS with horizons not analyzed (elemental loss extrapolated from other horizons).
(**) Composite PS (stacked PSs where the lower horizons of the upper PS overlap the upper horizons of the lower PS; Tabor and Myers, 2015).
Italicized PS samples reflect polygenetic or diagenetic overprinting of pedogenesis according to Hevia-Cruz et al. (2024a, 2024b), not considered for cation export and weathering estimates.

~ -4.6 to ~ 58 [10^6 Mol km^{-2} yr^{-1}]. Considering just Ca and Mg cations, elemental exports are ~ -36 to 1850 [t km^{-2} yr^{-1}] (or equivalently -0.7 to 35 [10^6 Mol km^{-2} yr^{-1}]). The full elemental export calculations can be found in Supplementary Table ST2.

4. Discussion

4.1. Paleosol geochemistry

In the next sections, we discuss the effects of major elements loss through the weathering of volcanic rocks. Consequently, we did not consider the PSs that incorporated allochthonous materials, as noted by Hevia-Cruz et al. (2024a, 2024b; profiles SM22H, Pi22B, Pi22H, and SM21E in Table 1), as those PSs formation comprise other processes not related to weathering. In addition, the profile SM21S has a negative cation export (Table 2), which is equivalent to elemental enrichment, probably due to the incorporation of extraneous volcanic ash. Thus, it is here also considered unsuitable for actual quantification of elemental loss by weathering processes. The incorporation of fresh materials, indeed, results in profile thicknesses and PS geochemistry that are not representative of *in situ* weathering of volcanic rocks, which might induce overestimated soil formation rates and inaccurate elemental fluxes. Using these screening criteria, nineteen profiles are discussed further (Table 2; Figs. 3, 4). For all the profiles, the lowermost sample corresponds to the fresh unweathered parental rock, except for profiles SM22J, SM21AA2, Pi22A, and SJ22A, which presented some indication of incipient weathering in the field and have greater LOI (Supplementary Table ST1). In those cases, the lowermost and least weathered sample was considered as the parental rock. Ti was preferred over Zr for determining tau values because it is more abundant, especially in basaltic rocks, as it is preferentially incorporated in basic lavas, which constitute most of the parental rocks included in this study (Hevia-Cruz et al., 2024a, 2024b).

All studied PSs show consistent Ti/Al and Ti/Zr ratios across profiles, supporting Ti immobility, except for profile SJ22A, which shows a decrease of Ti on its upper part (Supplementary Figure SF1; Nesbitt and Wilson, 1992). This Ti decrease could be related to organic complexation, fluctuating redox conditions, or particularly intense weathering (Du et al., 2012). The profile SJ22A yields the highest soil formation rate (Table 1), thus intense weathering could explain the sharp $\tau_{j,w}$ increase in the uppermost horizon, reflecting Ti loss instead of enrichment in other elements (Fig. 3).

Fig. 3 shows the $\tau_{j,w}$ of the selected PS profiles, where different behaviors can be observed, revealing several processes impacting the geochemistry of PSs. Ca and Mg generally show a depletion pattern, although addition is observed for the uppermost horizons of several profiles (SJ22C, SJ22A, SM21A), especially for Mg. This sharp variation is observed in the uppermost horizon of several profiles for all elements, potentially attributable to reworking during the emplacement of the overriding lava flow, which might have incorporated fresh materials into otherwise level substrate. This is particularly relevant for the profiles SM22C, SM21J, Fa22A, SJ22A, and especially for SJ22C where this seems to have reached ~30 cm depth. Profiles SM21A, SM21G, and SM22J show very low variability. In SM21AA2, most elements show low variability, Ca and Mg are slightly depleted, and Na is very enriched. K and Na are depleted in several profiles (SM21H, SM22E, Pi22D, Fa22D, SM21U, SM21AA1), but in other profiles, they are also enriched (Pi22F, Pi22J, Fa22A, Pi22A, SJ22A, except for the uppermost sample). This might be expected, as Na and K tend to be less mobile than Ca and Mg during weathering (Sheldon and Tabor, 2009, and references therein). Nevertheless, in some profiles, Na and K even show a pattern of addition (SM22C, SM21J, SM22B in its lower part). The Na addition is here attributed to the incorporation of sea salt aerosols, mainly constituted by sodium chloride (e.g., Cochran et al., 2017; Bertram et al., 2018). K variations are further discussed below.

Silicon is generally less depleted, reaching up to ~50 % loss in profiles SM22E, Fa22C, and SM21AA1, while Al, Fe and Mn tend to be more conservative, and even to accumulate in several profiles (SM22C, SM21J, Pi22F, Fa22A, Fa22D, SJ22C, Pi22A). This can be attributed to the precipitation of secondary minerals, as Al and Fe are incorporated into secondary minerals like kaolinite, gibbsite, and iron oxides (Chadwick et al., 2003), and Mn and Fe form oxides and hydroxides under common redox conditions in volcanic soils (Schwertmann and Taylor, 1989).

The variation in K concentrations might be impacted by organic activity (Jobbágy and Jackson, 2001), but K can also be incorporated into secondary clay minerals like illite (Berner and Berner, 2012). As Rb and K have similar geochemical behavior (Group (I) alkali metals) but vegetation uptakes preferentially K over Rb, vegetation probably impacted the K depletion during pedogenesis because τ_K values are lower than τ_{Rb} values in most PS profiles (Fig. 4). For those profiles for which K is enriched (e.g., SM21V, SJ22A), Rb is also enriched, pointing to the precipitation of clay minerals retaining K (Berner and Berner, 2012).

From the geochemistry of most profiles, we infer different processes associated with weathering, such as leaching and secondary mineral precipitation, although several profiles show some minor reworking in their upper parts, probably due to the emplacement of the overriding lava flow. However, Ca and Mg are just slightly impacted by addition in the uppermost horizons. Consequently, our estimates of weathering rates are not significantly impacted by these variations because any addition of elements would result in lower weathering rates, so our estimates of cation export are probably minimum values and could have been even greater.

Table 2
Cation export estimates based on the mass transfer function, density, thickness, parental rock composition, and maximum formation time of paleosols.

Profile	ρ [g cm^{-3}] of the parental rock	Weighted mean elemental loss (Ti immobile)								Parental rock composition [wt%]								Cation export [t km^{-2} yr^{-1}]	Ca + Mg export [t km^{-2} yr^{-1}]	Cation export [10^{6} Mol km^{-2} yr^{-1}]	Ca + Mg export [10^{6} Mol km^{-2} yr^{-1}]
		τ_{Si}	τ_{Al}	τ_{Fe}	τ_{Mn}	τ_{Mg}	τ_{Ca}	τ_{Na}	τ_{K}	SiO_2	Al_2O_3	Fe_2O_3	MnO	MgO	CaO	Na_2O	K_2O				
SM21H*	2.0	−0.2	−0.1	0.2	0.2	0.2	−0.5	−0.7	−0.5	41.7	17.5	15.9	0.2	4.5	6.1	2.2	1.0	99.4	163.0	2.2	0.9
SM22C	2.5	0.7	1.1	0.4	2.0	−0.4	−0.6	0.5	1.5	43.8	16.2	13.4	0.2	4.3	7.3	2.8	1.1	53.7	107.3	0.7	2.1
SM21J*	2.5	0.3	0.6	0.1	0.8	−0.3	−0.6	0.2	0.4	43.5	15.4	14.5	0.2	4.7	6.6	2.9	1.6	156.5	197.3	2.8	3.9
SM22E	2.5	−0.3	−0.1	0.1	0.1	−0.2	−0.5	−0.7	−0.8	46.5	13.2	12.4	0.2	7.8	9.4	2.4	1.4	969.3	672.3	21.6	13.3
Pi22D	2.5	−0.1	0.1	0.1	0.0	−0.1	−0.2	−0.3	−0.4	45.0	14.4	12.6	0.2	9.4	10.5	2.5	0.7	62.8	48.9	1.3	0.9
Pi22F	2.5	0.0	0.3	0.3	0.4	0.3	−0.4	−0.2	0.0	44.3	16.0	13.4	0.2	6.3	10.2	2.9	0.6	155.7	123.3	2.7	1.6
Pi22J	2.5	−0.1	0.0	0.0	0.1	−0.4	−0.6	−0.3	−0.1	44.0	15.3	13.1	0.2	6.2	11.0	2.2	0.6	754.8	704.0	15.6	14.0
Fa22A	2.5	−0.1	0.3	0.0	0.3	−0.3	−0.6	0.3	−0.1	39.0	17.6	14.9	0.2	2.7	5.6	3.7	1.1	173.6	219.4	2.7	4.2
Fa22C	2.5	−0.4	−0.2	0.0	−0.1	−0.8	−0.9	−0.4	−0.5	45.2	20.5	10.2	0.1	3.2	8.4	3.4	0.6	606.7	515.9	12.9	10.1
FA22D	2.5	−0.3	0.3	0.8	1.2	−0.6	−1.0	−0.7	−0.8	45.3	19.9	8.9	0.1	2.6	6.6	3.2	1.3	2642.5	1851.6	58.2	35.3
SJ22C	2.0	0.0	0.2	0.1	0.2	−0.4	−0.3	−0.1	−0.2	46.0	17.4	12.0	0.2	3.6	8.0	3.3	1.1	91.6	79.5	1.9	1.6
SM22B	1.0	0.0	−0.1	−0.1	0.0	−0.6	−0.4	0.1	0.0	55.5	19.0	6.1	0.1	1.9	1.5	4.2	4.0	166.1	206.3	3.5	4.6
SM21G*	1.0	0.1	0.1	0.0	0.1	0.0	0.2	−0.1	0.0	50.2	19.5	7.7	0.1	1.2	1.2	4.8	3.3	8.5	−3.6	0.3	−0.1
SM22J	1.0	−0.1	0.0	0.0	0.1	0.1	−0.1	0.0	−0.1	49.8	24.3	6.5	0.4	0.4	0.3	2.5	2.4	5.0	−0.4	0.1	0.0
SM21U & SM21V**	2.0	−0.4	−0.3	−0.1	−0.4	−0.3	−0.5	−0.5	−0.7	49.6	16.6	9.7	0.2	4.0	7.6	4.4	2.5	280.8	163.6	6.4	3.2
SM21AA**	1.4	−0.4	−0.2	−0.1	−0.3	−0.4	−0.5	0.3	−0.5	43.7	16.1	8.7	0.2	6.3	6.2	5.6	1.8	222.6	259.2	3.9	5.5
Pi22A*	2.0	−0.2	0.2	−0.1	0.1	−0.5	−0.4	0.1	−0.1	36.6	11.5	13.0	0.2	10.8	5.0	1.0	0.3	193.7	196.7	4.4	4.5
SJ22A	2.0	0.1	0.3	0.1	0.2	−0.2	−0.4	0.0	0.4	44.2	15.4	12.5	0.2	5.8	9.7	3.0	1.0	1641.1	1815.3	30.8	34.6
SM21A	1.0	0.0	−0.1	0.0	−0.1	0.1	0.0	−0.1	0.0	59.0	19.4	4.2	0.2	0.6	0.5	5.1	5.0	5.7	−2.1	0.2	0.0
*SM21S**	*2.0*	*0.2*	*0.2*	*0.2*	*0.4*	*0.0*	*0.3*	*0.2*	*0.2*	*60.8*	*17.8*	*4.8*	*0.2*	*0.9*	*1.6*	*5.6*	*4.7*	*−181.5*	*−36.1*	*−4.6*	*−0.7*

São Miguel (SM) age data from Hevia-Cruz et al. (2024a).
Pico (Pi), Faial (Fa), and São Jorge (SJ) age data from Hevia-Cruz et al. (2024b).
(*) PS with horizons not analyzed (elemental loss extrapolated from other horizons).
(**) Composite PS (stacked PSs where the lower horizons of the upper PS overlap the upper horizons of the lower PS; Tabor and Myers, 2015).
Italicized samples reflect polygenetic or diagenetic overprinting of pedogenesis.
In several cases, the Ca + Mg export is greater than the total cation export, due to Na and/or K addition (see main text for further discussion).

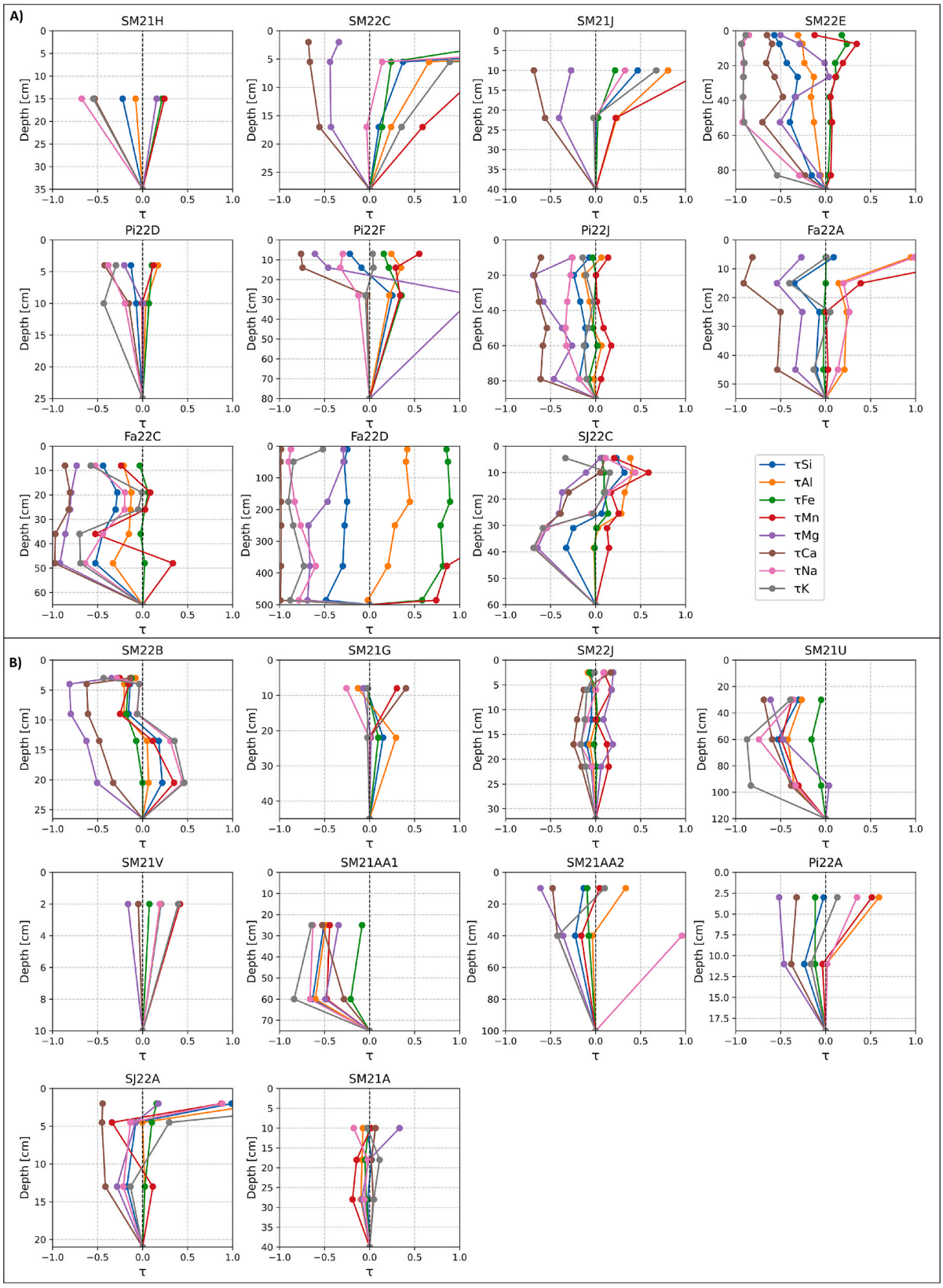

Fig. 3. Mass transfer function of major elements in the paleosols studied in this work, considering Ti as an immobile element. A) shows the paleosols developed in lava flows (PS type I) and B) shows those developed on pyroclastic deposits (PS types II and III).

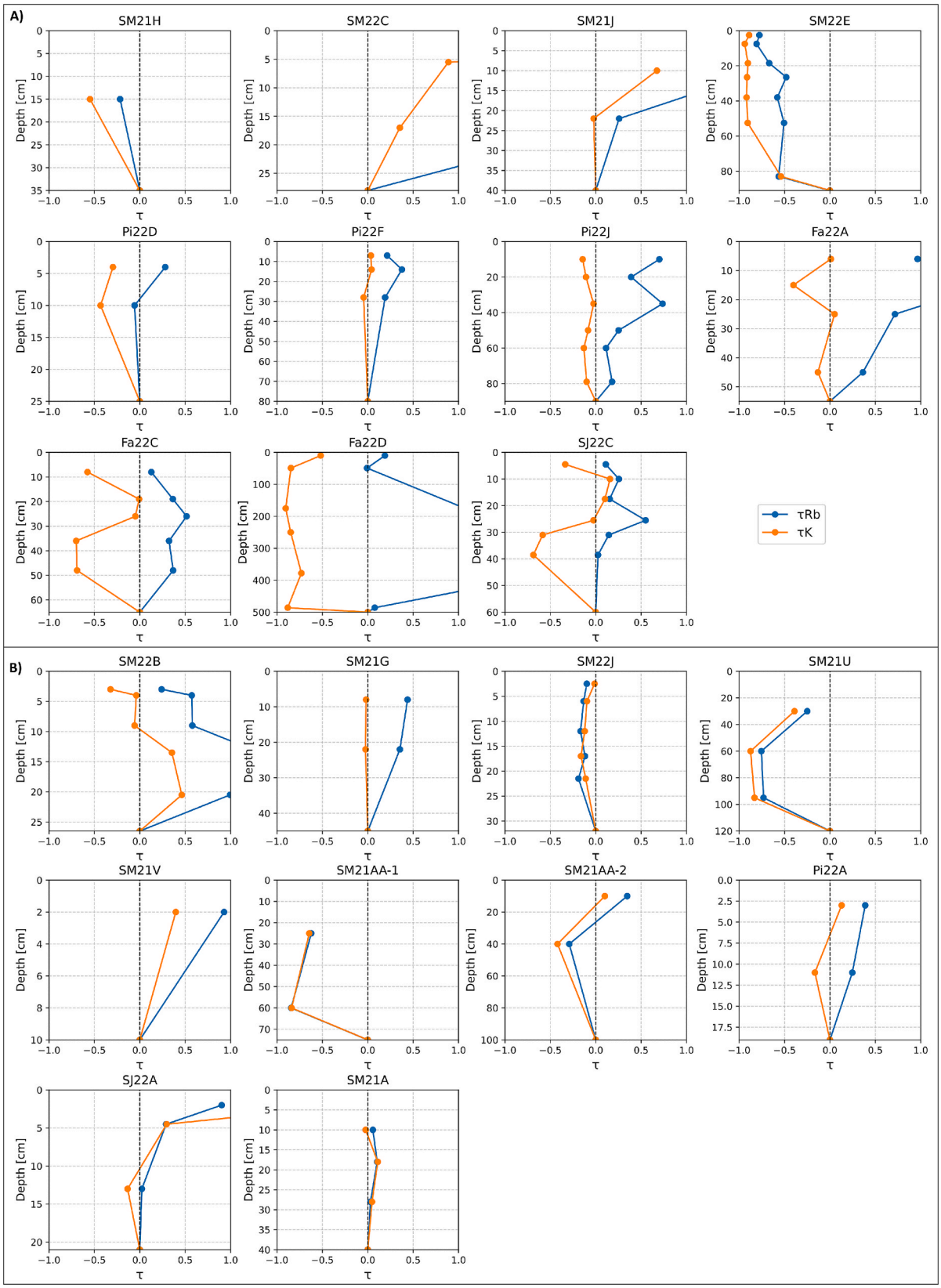

Fig. 4. Mass transfer function of Rb and K with Ti as an immobile element. A) shows the paleosols developed in lava flows (PS type I) and B) shows those developed on pyroclastic deposits (PS types II and III).

4.2. Intense soil production and paleo-weathering rates

In the profiles studied in this work, the PS formation time does not seem to be directly correlated to the nature and texture of the initial volcanic deposit (PS types I to III). This is the case even for Fa22D, which is particularly thick (Fig. 5A, B). The weathering degree is here represented by the index bases/alumina in Fig. 5C–D. The sum of bases (Ca, Mg, Na, K) over alumina is a commonly used metric for the degree of chemical weathering, where values approaching 0 reflect near total destruction of feldspars and values over ~2 reflect unweathered basalt (Sheldon, 2003; Sheldon and Tabor, 2009). We calculated the bases/alumina weathering index for the B horizon of each PS to compare the maximum weathering degree with different parameters. B horizons were preferred over other horizons because they typically record the highest degree of weathering, i.e., lower bases/alumina (Sheldon and Tabor, 2009; Hevia-Cruz et al., 2024a, 2024b). In our case, bases over alumina neither seem to be related to profile thickness, PS type, maximum formation time, or soil formation rate (Fig. 5C–F), suggesting that the degree of chemical weathering is mostly driven by climatic and environmental conditions, as previously discussed by Hevia-Cruz et al. (2024b). Nevertheless, the thickness of the PS correlates well with the maximum PS formation time (Fig. 5G), as expected, because a longer

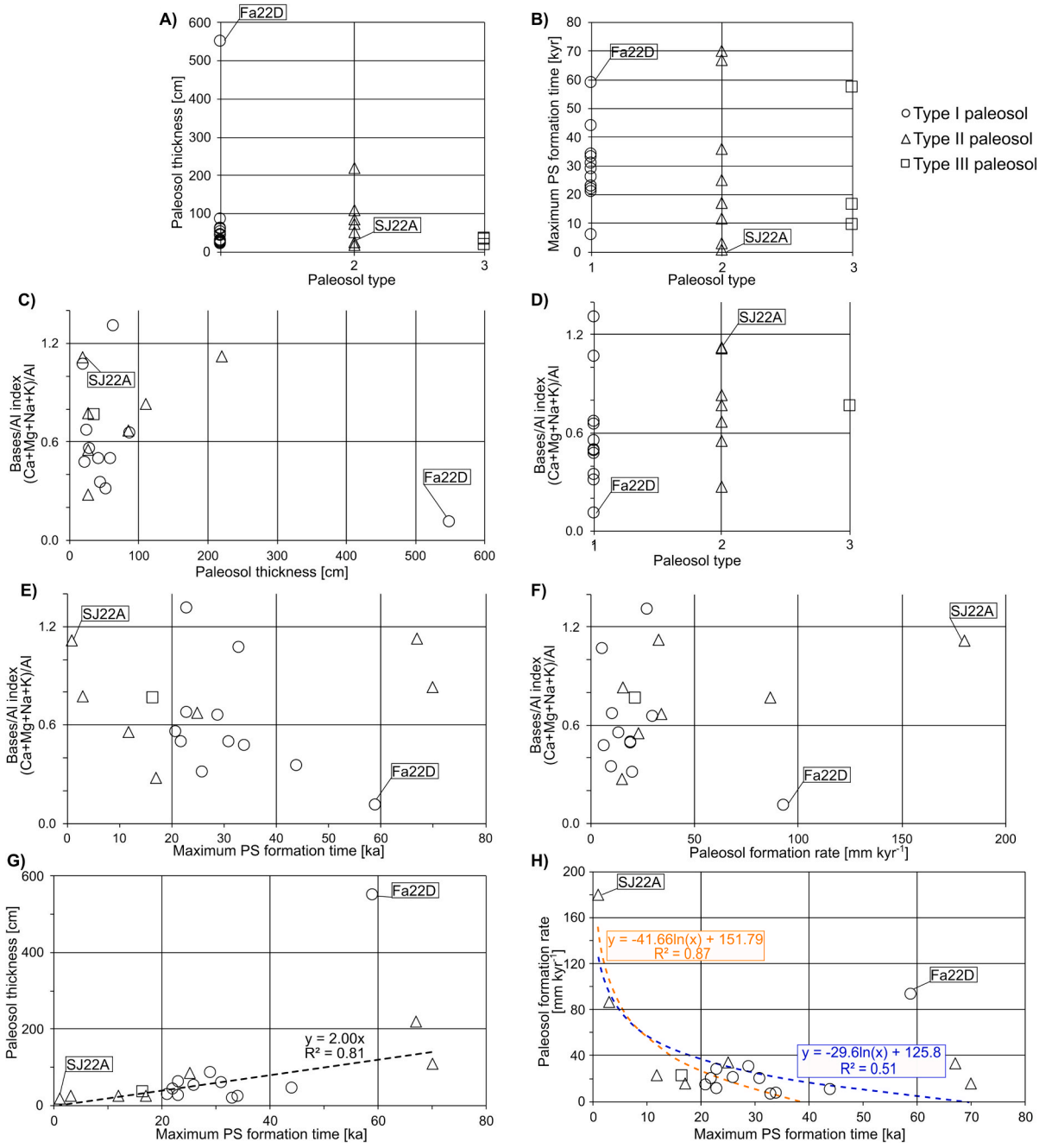

Fig. 5. Relationships between paleosol characteristics (type, thickness, formation time, weathering degree and formation rate). A) paleosol thickness by type of paleosol; B) maximum paleosol formation time by type of paleosol; C), D), E) and F) weathering degree (Bases/Al index; concentrations of each oxide in wt. %/molecular weight) compared to paleosol thickness, type, formation time, and rate; G) paleosol thickness compared to maximum formation time. The dashed line represents paleosol thickness as a linear function of formation time; H) paleosol formation rate vs formation time, the blue and orange dashed curves relate the paleosol formation rate and formation time with a logarithmic function, with and without the three data with higher PS formation time (blue and orange dashed lines, respectively).

weathering duration allows for the weathering front to reach greater depths as porosity develops in a context of limited erosion.

Our soil formation rate estimates are high, comparable to those obtained by Dosseto et al. (2022) for the tropical volcanic island of La Réunion based on U-Th series dating of three soil profiles. Although our soil production estimates are generally lower than those at La Réunion, our data also point to a high soil production rate during short periods of intense weathering (Table 1; Fig. 5H). In contrast to La Réunion (Dosseto et al., 2022), we did not study weathering profiles developed cumulatively over periods as long as 1 Myr in the Azores. Thus, our relatively high estimation of soil production might be related to the different precipitation regimes of these two volcanic settings, or simply to a better-resolved period of actual soil formation, or a combination of both. Current mean annual precipitation at La Réunion is between 1000 and 3500 [mm yr^{-1}] in the study sites of Dosseto et al. (2022), but up to 12,000 [mm yr^{-1}] (Meteo France, 2022), while the Azores study sites reach just ~960 to 1100 [mm yr^{-1}] of annual precipitation (AEMET & IM, 2012). This more than twice precipitation difference could promote deeper weathering fronts, although differences in moisture regimes were not necessarily the same over the past 1 Myr. Indeed, Hevia-Cruz et al. (2024b) observed fast floral humidity province changes in the Azores that tracked deglacial events, reaching rainforest conditions at ~110 ka on São Miguel Island.

In terms of weathering rates, our estimates are higher than cation exports deduced from modern river geochemistry in the Azores (Fig. 6; Louvat and Allègre, 1998), but similar to estimates from La Réunion Island (Louvat and Allègre, 1997). Extending elemental fluxes associated with weathering from soil to watershed scale requires caution, as discrepancies have been widely discussed, often showing higher rates at smaller scales (e.g., Schnoor, 1990; Brantley, 1992; White et al., 1996). Navarre-Sitchler and Brantley (2007) identified lower rates at the watershed scale and higher rates at lower spatial scales, although their work includes a single soil scale study, limiting direct comparisons with our reconstructions. Other studies have reported decreasing activation energies for weathering at broader scales (Brantley et al., 2023), or similar rates across scales (Engel et al., 2016), while Egli et al. (2014) showed that different methodologies yield varying soil formation rates. In volcanic contexts, weathering rates at the clast scale (e.g., Pelt et al., 2008; Sak et al., 2018) tend to be lower than our estimates, likely due to their focus on massive volcanic clasts. We propose that this discrepancy is not related to spatial scale, but to the temporal constraints of the weathering process. For instance, White and Brantley (2003) highlighted weathering duration as a key variable of weathering dynamics. Unlike studies with longer weathering intervals (Dosseto et al., 2022; Zehetner et al., 2024), our geochronology provides tightly constrained timeframes, leading to higher soil formation/weathering rates. This difference arises from the longer time gap between parental rock formation and the present, as past studies lacked a younger age limit.

Moreover, the paleo-weathering rates here obtained might be underestimates of actual weathering fluxes. Our weathering estimates, indeed, assume an isotropic volcanic substrate and were extended to the whole archipelago, but actual rates probably varied as well with texture and localized disturbance (e.g., landslide) history. Soils modify infiltration and water–rock interaction (Perez-Fodich et al., 2024), while vegetation enhances regolith production through root-driven fracturing (e.g., Hasenmueller et al., 2017), and organic activity alters acidity and redox conditions (Drever and Stillings, 1997). In consequence, weathering was likely higher on exposed surfaces (Emberson et al., 2016) and enhanced by biological activity, and reduced under stable, soil-covered areas. Consequently, our estimates are conservative (e.g., unaccounted eroded material, use of maximum formation time, conservative parent material density, stable PS locations, parental rock covered by soil or vegetation), suggesting potentially higher paleo-weathering rates. Even halving the conservative parental rock densities assumed in section 3.2, past weathering rates in the Azores align with those of modern tropical volcanic islands. These high cation export rates, driven by intense weathering during soil formation, also imply a substantial potential for atmospheric CO_2 drawdown, which is further discussed in section 4.5.

4.3. Rapid decrease of soil production and weathering intensity

Interestingly, our estimates of PS formation rate and maximum formation time indicate a rapid decrease in soil production rate after only a few kyr (Fig. 5H). Two PSs (SJ22A, SM22B) show very high formation rates (> 80 mm kyr^{-1}), associated with very short maximum soil formation time (< 3 kyr; Table 1, Fig. 5). Inaccurate age control is unlikely because Hevia-Cruz et al. (2024a, 2024b) obtained reproducible ages for the volcanic units bracketing both profiles. Adding the other data points suggests an overall logarithmic decrease of soil formation rates through time. Soil production rates become constant and relatively low (< 40 mm kyr^{-1}) after only 10 kyr, getting close to zero after ~35 kyr (orange dashed line in Fig. 5H), and with minimal exceptions after a period of ~60 kyr (Blue dashed line in Fig. 5H). This net soil production reflects the balance between weathering front deepening and denudation. While a non-eroding system could theoretically reach zero alteration, this is rarely observed. Soil production likely stabilizes at low, quasi-stationary values similar to denudation rates, though our data are insufficient to confirm this. However, the high soil production during the first ~35 kyr of formation stands out as a key finding. Further studies, for example in other islands of the Azores or on other volcanic islands, could help to elucidate if this temporal threshold is a general rule or if local edaphic factors impact the duration after which soil production rate becomes negligible. Zehetner et al. (2020, 2024) observed rapid changes in soil coverage and elemental loss in the Galapagos Islands for soils older than ~26 ka, leading to a decrease in soil production. This timeframe is consistent with our data, as we considered the maximum time for soil formation. It is worth noting that their study took place in a wetter environment and does not consider fluctuations in the environmental conditions, e.g., during sharp glacial-interglacial variations over the past 1 Myr.

The decrease in weathering rate is less clear than that of soil production, as one single profile (Fa22D) has a long maximum formation time, but also very high thickness and weathering degree (Supplementary Figure SF2). The decreases in soil formation and weathering rates are probably a consequence of cation depletion on primary phases and precipitation of secondary clay minerals, and Fe- and Al-oxides that are immobile under most pH conditions (further discussed in section 4.4).

4.4. Extreme weathering during interglacial peaks

Our estimates of weathering rates, expressed as cation exports in Fig. 6, are much higher than the cation exports observed by Louvat and Allègre (1998) based on modern river geochemistry on São Miguel Island, but comparable to and sometimes even greater than cation exports estimated from modern river geochemistry at La Réunion Island (Fig. 6A; Louvat and Allègre, 1997). Using the weathering law for basalts of Dessert et al. (2003; $Cation\ export\left[kg\ km^{-2}yr^{-1}\right] = MAP\left[mm\ yr^{-1}\right] * 6.69 * e^{(0.0677 * MAAT[^{\circ}C])}$) with paleoprecipitation and paleotemperatures reconstructions during interglacial peaks after Hevia-Cruz et al. (2024a, 2024b) gives cation exports of up to ~65 [t km^{-2} yr^{-1}] (Supplementary Table ST3), which is still much lower than the mean of ~400 [t km^{-2} yr^{-1}] that we obtain from the PSs geochemistry (Table 2; Fig. 6A). Without considering the outliers (values over 1000 [t km^{-2} yr^{-1}], not shown in Fig. 6A), our mean cation export is over 200 [t km^{-2} yr^{-1}], more than three times the estimates from basalt weathering laws of Dessert et al. (2003) and four times the highest value obtained by Louvat and Allègre (1998) from modern river geochemistry in São Miguel.

These extremely high weathering export estimates point to periods of environmental conditions in the geologic past particularly favorable for weathering to occur efficiently, which can explain the pulses of soil

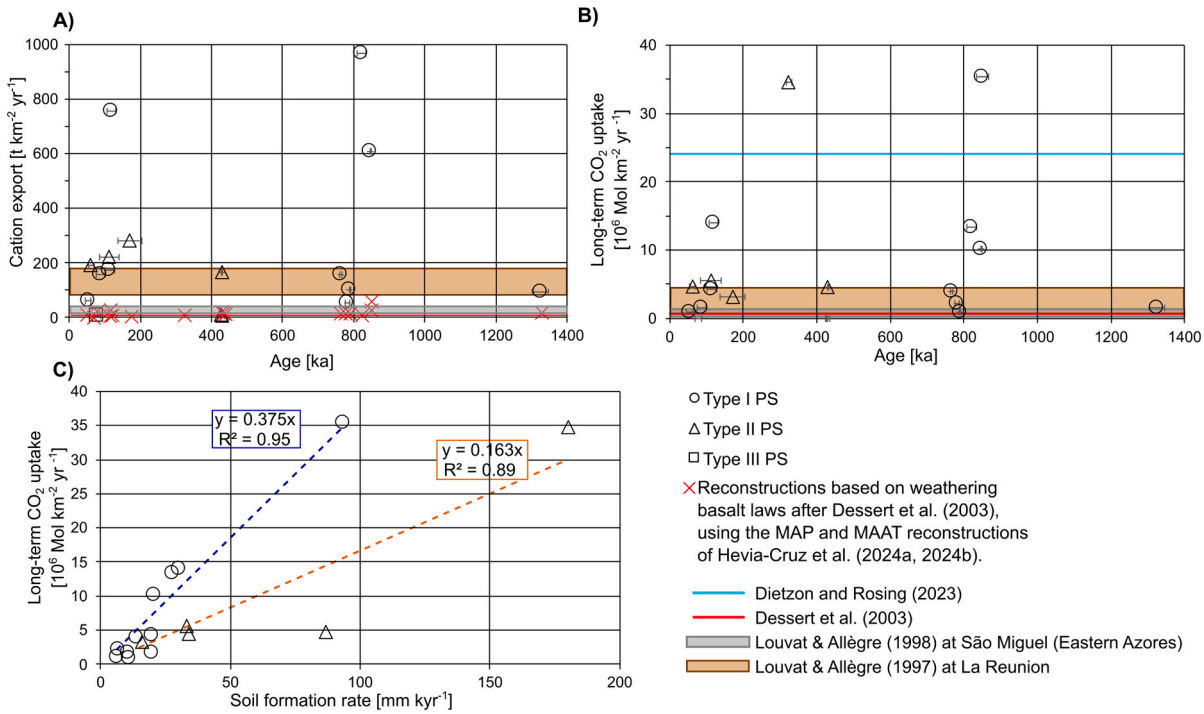

Fig. 6. Cation export and equivalent long-term atmospheric CO_2 uptake rates. A) Cation export estimates over the past 1400 ka. The gray area represents the cation export reported by Louvat and Allègre (1998) for São Miguel Island, the brown area is the cation export reported by Louvat and Allègre (1997) for La Réunion Island, and the red crosses are the reconstructed values after the basalt weathering laws of Dessert et al. (2003), using the temperature and precipitation reconstructions of Hevia-Cruz et al. (2024a, 2024b). The red line corresponds to the present values reported in Dessert et al. (2003); B) long-term CO_2 uptake over the past 1400 ka. The light blue line corresponds to an estimate of CO_2 uptake by fine-grained glacial till of granitic origin in Denmark (Dietzen and Rosing, 2023), the gray area corresponds to the range of CO_2 uptake reported by Louvat and Allègre (1998) from modern river geochemistry on São Miguel Island, the brown area corresponds to that of La Réunion Island by Louvat and Allègre (1997), and the red line is a CO_2 uptake estimate from basalt weathering after Dessert et al. (2003), using present-day precipitations and temperature (AEMET and IM, 2012; Hernandez et al., 2016); C) long-term CO_2 uptake as a function of soil formation rate, with a linear function relationship for type I and type II PSs (blue and orange dashed line, respectively).

formation described in Hevia-Cruz et al. (2024a, 2024b). Notably, the values here obtained from PSs in the Azores are comparable to cation exports observed by Louvat and Allègre (1997) from modern rivers at La Réunion tropical island, suggesting that near tropical conditions were reached in the Azores during interglacial periods. This is also consistent with floral humidity province reconstructions by Hevia-Cruz et al. (2024b) that support tropical vegetation at the time. Under such conditions, the rapidly decreasing rate of weathering (see 4.3) suggests these high cation exports were briefly (few kyr) sustained by the fast deepening of the weathering front into the parental rock, a process that, according to our data, became very rapidly inefficient over time (Fig. 5H).

The relatively fast weathering estimated for the profile Fa22D compared to other type I PSs (2640 [t km^{-2} yr^{-1}], Table 2) can be explained by its alkali feldspar-rich parental rock (up to ~50 %), which is very easy to weather. In addition, it is in a fault zone (Hildenbrand et al., 2012), which might have promoted rock fracturing, increasing its permeability and favoring persistent rainwater infiltration. In the case of profile SJ22A, as well as for soil formation rate, the extremely high weathering rate (1640 [t km^{-2} yr^{-1}], Table 2) could be due to the very short maximum soil formation time (1 kyr; Figs. 5, 6), for which inaccurate age control is unlikely. Finally, the profile SM22E does not seem to be affected by particular local factors, but it should be interpreted with care, as it far exceeds the limit of soil production rate proposed by Dixon and von Blanckenburg (2012) of up to 450 [t km^{-2} yr^{-1}] for predominantly lowland settings. However, it is worth noting that this limit has also been surpassed in other mountainous settings, easily reaching over 800 to 2000 [t km^{-2} yr^{-1}] in the Alps (Egli et al., 2014).

The difference between our estimates of the weathering rate and those of Louvat and Allègre (1998) may arise from São Miguel's eastern regions having older bedrock (Fig. 1B), because weathering rates decline with substrate age (e.g., Rad et al., 2011; Börker et al., 2019; Dosseto et al., 2022; Zehetner et al., 2024). The initial fast weathering of fresh bedrock is a transient process, and so the basalt weathering laws presumably reflecting steady-state denudation do not capture the initially intense weathering revealed by our tight geochronological constraints. Rainwater interacting with pre-weathered substrates likely reduced leaching, lowering cation exports. This is particularly the case for non-eroding soils, as the weathering front requires supply of water, oxygen, and CO_2 to propagate downwards, which quickly decrease as the profile thickens (e.g., Gabet and Mudd, 2009; West, 2012; von Blanckenburg et al., 2021). This is probably the case of our reconstructions, as the studied PSs developed in low slope areas, where erosion was limited (Hevia-Cruz et al., 2024a, 2024b). Other processes may also contribute to this discrepancy, as perennial river studies underestimate exports during extreme events or as underground flows, which may account for an important percentage of cation fluxes (e.g., Hildenbrand et al., 2005; Clow and Mast, 2010; Schopka and Derry, 2012).

In summary, the discrepancy between our PS-based estimates and those inferred from modern river chemistry is primarily due to two factors: warmer/wetter interglacial peaks, as evidenced by paleoenvironmental reconstructions (Hevia-Cruz et al., 2024b) and soil formation/weathering rates (comparable to modern tropical settings); and modern river-based estimates likely underestimating weathering due to unaccounted ephemeral and underground flows. This supports the recurrence of such tropical conditions in the Azores throughout the late Quaternary, promoting pulses of intense weathering.

This study, as well as those of Hevia-Cruz et al. (2024a, 2024b), did not identify PSs formed during glacial periods in either the Central or Eastern Azores. Comparing the weathering rates obtained here with

those from glacial periods would provide valuable insights into the variability of weathering dynamics throughout glacial–interglacial cycles in the Late Quaternary. To address this, future fieldwork should specifically target the identification and sampling of PSs formed during glacial intervals.

4.5. Impact on past atmospheric CO_2 uptake

These high weathering rates probably had a great impact on the carbon cycling through the uptake of atmospheric CO_2. Silicate weathering can be expressed as:

$$Silicate + 2CO_2 + 3H_2O \Leftrightarrow Cation^{2+} + 2HCO_3^- + secondary\ minerals$$

The dissolved bicarbonate (HCO_3^-) and cations (Ca^{2+}, Mg^{2+}) are carried in solution, assuming they are not incorporated into secondary minerals. This stoichiometry indicates that each cation captures two atmospheric CO_2 molecules. However, half of this CO_2 is released back to the atmosphere–ocean system during the precipitation of carbonates via the equation (Berner et al., 1983; Berner, 2003):

$$Ca(Mg)^{2+} + 2HCO_3^- \Leftrightarrow Ca(Mg)CO_3 + H_2O + CO_2.$$

with the term (Mg) a proportion between 0 and 1 of Mg replacing Ca. Thus, we can consider that each cation of Ca^{2+} and Mg^{2+} exported is equivalent to the same amount of CO_2 consumed from the atmosphere, i.e., equivalent to the right column of Table 2 (Fig. 6B, 6C; Supplementary Table ST2). Fig. 6B shows that our long-term atmospheric carbon uptake estimates are generally higher than those previously reported in São Miguel Island (Louvat and Allègre, 1998; Dessert et al., 2003), following the observed mismatch between the weathering rates obtained by these authors and our data (see section 4.2). Comparing our CO_2 consumption rate estimates with global data also points to particularly high CO_2 uptake in the Azores at the time when the studied PS were formed. For instance, our estimates are in the higher range of consumption rates in the review of Li et al. (2016), similar to modern active volcanic settings under tropical conditions (Supplementary Figure SF3 and their Table 1). The high rates obtained in our work are probably related to the highly reactive chemistry and the high specific surface area of the parental materials being weathered. Indeed, types II and III PSs have developed from pyroclastic deposits, while type I PSs have developed from the brecciated upper parts of lava flows. The latter shows very sharp contacts (Milne et al., 1995) with the fresh unweathered parental lava flows, highlighting the influence of fracturing and vesicularity on the kinetics of weathering. Our estimates are generally lower than those associated with the weathering of very fine-grained glacial till from granitic origin (Dietzen and Rosing, 2023), probably due to an even higher specific surface area. The only exceptions are Fa22D, probably due to its high feldspar content and the local tectonics (see 4.4), and SJ22C, which might be related to its extremely short maximum formation time (ca. 1 kyr), which is in line with the observations of Zehetner et al. (2024) in the Galapagos, where they obtained the greater elemental losses in the youngest soil profiles (< 4.3 ka).

However, changes in the surface composition and texture over time also control the rate of CO_2 consumption. For the Azores, while both the long-term weathering and equivalent CO_2 consumption rates seem to be related to the soil formation rate, their relationship is different in lava flows and pyroclastic deposits (Fig. 6C). This can be explained by the higher density of lava flows, which sustained a high cation export without a deep weathering front. In turn, less dense pyroclastic deposits with higher specific surface area may deplete faster, thus requiring a greater degree of vertical profile development to sustain high cation export and consequent CO_2 uptake.

It is worth noting that, in the present context of additional (and increasing) anthropogenic emissions, an increase in silicate weathering will not be efficient enough to counteract the increased atmospheric CO_2 concentration. Even considering the highest CO_2 uptake among our estimates (1850 [t km^{-2} yr^{-1}]; Table 2), and extrapolating it to the full surface of the Azores Archipelago (2322 km^2; Cruz and Soares, 2018), it represents a total of almost 4.3 10^6 [t yr^{-1}] of atmospheric CO_2 consumption. This represents nearly 0.01 % of the yearly human emissions just from fossil fuels (37 10^9 [t yr^{-1}] of global emission; Ritchie and Roser, 2020), which is negligible. Gaillardet et al. (1999) estimated a total global carbon consumption by weathering (silicate and carbonate) of 0.288 10^9 [t yr^{-1}] of C, equivalent to ca. 1.06 10^9 [t yr^{-1}] of CO_2. If one considers an extreme 10 times increase of this global CO_2 consumption (the highest increase we deduced for interglacial periods compared to present estimates from river chemistry), it would represent less than a third of the annual human emissions. In consequence, geoengineering projects, including enhanced weathering strategies, need to consider the small proportional impact that these projects can have and the long time scales of these processes (e.g., Colbourn et al., 2015).

4.6. Broader implications, challenges, and perspectives

Our study shows that weathering and associated atmospheric CO_2 consumption on volcanic islands are not steady-state processes. On the contrary, they are transient (pulsed) processes (for example, see Fig. 2 in Hevia-Cruz et al., 2024b), which occur intensively over timescales of only a few kyr to a few tens of kyr under climatic conditions that are warm and wet enough for chemical lixiviation and cation mobilization to initiate and propagate. In the Azores, at least three Quaternary interglacial stages appear to represent favorable periods where sufficiently high temperatures and mean annual precipitation have been reached to trigger episodic weathering and potential climatic feedback through enhanced atmospheric CO_2 consumption. The average weathering rates here estimated around these glacial peaks suggest variable but overall decreasing velocity of weathering over only a few millennia. However, the exact dynamics of (paleo-) sols development requires further investigation, e.g., through systematic U-Th studies on PS profiles. Such efforts may be useful to refine the equations of existing weathering laws, and to assess the variations in cation export rates and associated carbon sequestration over different timescales better. It would also be interesting to study and determine weathering laws on differentiated volcanoes. They frequently have explosive eruptions, producing fine-grained deposits with much higher specific surface area (e.g., Papelis et al., 2003; Delmelle et al., 2005) and dispersal, and are thus potentially more susceptible to enhanced weathering and fast CO_2 consumption. In the Azores, the relative scarcity of differentiated volcanic deposits such as trachytic fallout prevents the systematic study of weathering and soil formation on these materials. The few examples observed on São Miguel were affected by recent contamination or were not well-constrained in time.

Finally, extrapolating the impacts of such fast weathering at larger scales remains challenging, as significant regional differences in past air moisture and temperature may have prevailed, even during globally warm and wet paleoclimatic periods. In this respect, PSs represent a unique record that can be used to jointly investigate the causal links between past atmospheric conditions, weathering and the eventual feedback effects on global climate (e.g., through intense CO_2 consumption). The increase in weathering rates inferred here may seem minor in the context of today's high CO_2 emissions. However, in a pre-industrial setting, such a shift could have significantly influenced atmospheric CO_2 levels and global paleoclimate, potentially accelerating transitions to glacial stages. Estimating the amount of atmospheric CO_2 consumed by weathering processes in the past remains challenging, as it relies on the assumption that the rates here calculated (per unit surface and time) can be up-scaled to the total surface of the islands at each period of interest. This is in most cases not directly verifiable, as individual weathered horizons were extensively buried by subsequent volcanism. Nevertheless, some of the PSs here studied can be traced over large distances within recent coastal cliffs, supporting major events of weathering over large areas. If similar weathering intensification occurred in other volcanic regions, its role in cooling Earth's atmosphere may have been greater than previously estimated. As such, extension of the present research topic to Late Quaternary volcanoes worldwide

represents a very promising line of research for the near future.

5. Conclusions

The combination of paleosols' physical characteristics, their geochemistry, and their precise geochronological constraints allowed us to estimate their formation rates, as well as cation loss and associate atmospheric CO_2 uptake during snapshots of soil formation over the past 1 Myr. Our work highlights the importance of thorough geochronological control to properly constrain the overall dynamics of past episodes of weathering and the associated CO_2 consumption.

Our estimates of soil formation rates reached similar values to soils formed on the tropical volcanic island of La Réunion. Thicker paleosols took longer to form, as longer formation time allows the weathering front to reach deeper into the parental rock. Soils formed rapidly during the first 20 to 30 kyr of pedogenesis, after which soil formation rates decreased to near zero. Further studies on other islands could help to elucidate if this is a general rule or if local factors impact the amount of time after which soil production becomes negligible.

PSs have generally developed faster on pyroclastic deposits than on lava flows. However, PSs on lava flows required less vertical development to maintain high cation exports due to their higher density. PS-based cation export estimates were higher than previous estimates based on the geochemistry of modern rivers in São Miguel Island (Eastern Azores). This is probably explained by hotter/warmer past conditions in the Azores during interglacial peaks, but also due to unaccounted weathering exports such as underground flow and ephemeral rivers. Associated atmospheric CO_2 consumption was also high compared to previous estimates, which suggests that the weathering of volcanic islands made a small, but significant contribution to global carbon sequestration during glacial-interglacial stages over the past 1 million years, possibly favoring subsequent cooling. It is worth noting that an extreme tenfold increase in CO_2 sequestration through weathering at the global scale would represent less than a third of human emissions from fossil fuels. We expect that future research in the North Atlantic region (e.g., Canary Islands, Cape Verde) and at broader scale (e.g., Large Igneous Provinces or the Andes) will determine if our high CO_2 uptake estimates were a local phenomenon or reached a global scale, and how such processes could impact global climate.

CRediT authorship contribution statement

Francisco Hevia-Cruz: Writing – review & editing, Writing – original draft, Visualization, Validation, Methodology, Investigation, Data curation, Conceptualization. **Anthony Hildenbrand:** Writing – review & editing, Writing – original draft, Visualization, Validation, Supervision, Project administration, Methodology, Investigation, Funding acquisition, Conceptualization. **Nathan D. Sheldon:** Writing – review & editing, Writing – original draft, Visualization, Validation, Supervision, Methodology, Investigation, Conceptualization. **François Chabaux:** Writing – review & editing, Writing – original draft, Validation, Investigation. **Fernando O. Marques:** Writing – review & editing, Writing – original draft, Validation, Investigation. **Julie Carlut:** Writing – review & editing, Writing – original draft, Investigation.

Data availability

Data are available through Mendeley Data at https://doi.org/10.17632/fdzjhb26wz.1.

Declaration of competing interest

The authors declare that they have no known competing financial interests or personal relationships that could have appeared to influence the work reported in this paper.

Acknowledgments

This work was supported by the CNRS-INSU TelluS-SYSTER program 2022-2023. We thank three anonymous reviewers who made important and constructive comments, greatly helping to improve this work. F.H-C. thanks to the French MESRI program (2020-2023) and the Graduate School Géosciences Climat Environnement Planètes for doctoral funding. We also thank Gaël Monvoisin and Frédéric Haurine for their help with geochemical analyses, and Valerie Godard for thin section preparation. This is LGMT contribution number 197.

Appendix A. Supplementary material

The Supplementary Material includes three figures and three tables. Supplementary Figure SF1 provides variations of immobile element ratios along paleosol profiles, Supplementary Figure SF2 contrasts paleosol-based weathering rate and formation time, and Supplementary Figure SF3 contrasts our estimates of atmospheric CO_2 consumption rates with those in the review of Li et al. (2016) from different volcanic settings. The Supplementary Tables ST1 to ST3 correspond to the full data used in this work, including the profile locations, descriptions, the ages used to constrain their ages and formation timing, and their major element geochemistry; the full calculation of weathering rates as elemental fluxes; and the equivalent atmospheric CO_2 uptake contrasted with that of the basalt weathering laws of Dessert et al. (2003). Supplementary Tables ST1 and ST2 are provided as separate files because of their sizes. Supplementary material to this article can be found online at https://doi.org/10.1016/j.gca.2025.05.035.

References

Ackerer, J., Chabaux, F., van Der Woerd, J., Viville, D., Pelt, E., Kali, E., Lerouge, C., Ackerer, P., di Chiara Roupert, R., Négrel, P., 2016. Regolith evolution on the millennial timescale from combined U–Th–Ra isotopes and in situ cosmogenic 10Be analysis in a weathering profile (Strengbach catchment, France). Earth Planet. Sci. Lett., 453, 33–43.

AEMET & IM, 2012. Atlas Climático de los Archipiélagos de Canarias, Madeira y Azores. Agencia Estatal de Meteorología de España e Instituto de Meteorología de Portugal.

Berner, R.A., 2003. The long-term carbon cycle, fossil fuels and atmospheric composition. Nature 426 (6964), 323–326.

Berner, R.A., Lasaga, A.C., Garrels, R.M., 1983. Carbonate-silicate geochemical cycle and its effect on atmospheric carbon dioxide over the past 100 million years. Am. J. Sci., 283 (7).

Berner, R.A., Kothavala, Z., 2001. GEOCARB III: a revised model of atmospheric CO2 over Phanerozoic time. Am. J. Sci., 301 (2), 182–204.

Berner, E.K., Berner, R.A., 2012. Global Environment: Water, Air, and Geochemical Cycles. Princeton University Press.

Bertram, T.H., Cochran, R.E., Grassian, V.H., Stone, E.A., 2018. Sea spray aerosol chemical composition: elemental and molecular mimics for laboratory studies of heterogeneous and multiphase reactions. Chem. Soc. Rev., 47 (7), 2374–2400.

Booth, A.M., Buma, B., Nagorski, S., 2022. Effects of landslides on terrestrial carbon stocks with a coupled geomorphic-biologic model, Southeast Alaska, United States. J. Geophys. Res.-Biogeosci., e2022JG007297.

Börker, J., Hartmann, J., Romero-Mujalli, G., Li, G., 2019. Aging of basalt volcanic systems and decreasing CO2 consumption by weathering. Earth Surf. Dyn., 7 (1), 191–197.

Boulad, A.P., Muller, J.P., Bocquier, G., 1977. Essai de détermination de l'âge et de la vitesse d'altération d'un sol ferrallitique camerounais à l'aide de la méthode du déséquilibre radioactif uranium–thorium. Sci. Géol. Bull., 30 (3), 175–188.

Brantley, S.L., 1992. Kinetics of dissolution and precipitation—experimental and field results. In: Kharaka, Y., Maest, A. (Eds.), Water–rock Interaction, vol. 7. Park City, pp. 465–469.

Brantley, S.L., Shaughnessy, A., Lebedeva, M.I., Balashov, V.N., 2023. How temperature-dependent silicate weathering acts as Earth's geological thermostat. Science 379 (6630), 382–389.

Brimhall, G.H., Dietrich, W.E., 1987. Constitutive mass balance relations between chemical composition, volume, density, porosity, and strain in metasomatic hydrochemical systems: results on weathering and pedogenesis. Geochim. Cosmochim. Acta 51 (3), 567–587.

Carmichael, R.S., 2017. Practical Handbook of Physical Properties of Rocks and Minerals (1988). CRC Press.

Chabaux, F., Blaes, E., Stille, P., di Chiara Roupert, R., Pelt, E., Dosseto, A., Ma, L., Buss, H.L., Brantley, S.L., 2013. Regolith formation rate from U-series nuclides: Implications from the study of a spheroidal weathering profile in the Rio Icacos watershed (Puerto Rico). Geochim. Cosmochim. Acta 100, 73–95.

Chadwick, O.A., Gavenda, R.T., Kelly, E.F., Ziegler, K., Olson, C.G., Elliott, W.C., Hendricks, D.M., 2003. The impact of climate on the biogeochemical functioning of volcanic soils. Chem. Geol., 202 (3–4), 195–223.
Chadwick, O.A., Chorover, J., Chadwick, K.D., Bateman, J.B., Slessarev, E.W., Kramer, M., Thompson, A., Vitousek, P.M., 2022. Constraints of climate and age on soil development in Hawai 'i. In: Biogeochemistry of the Critical Zone. Springer International Publishing, Cham, pp. 49–88.
Clow, D.W., Mast, M.A., 2010. Mechanisms for chemostatic behavior in catchments: Implications for CO2 consumption by mineral weathering. Chem. Geol., 269 (1–2), 40–51.
Cochran, R.E., Ryder, O.S., Grassian, V.H., Prather, K.A., 2017. Sea spray aerosol: The chemical link between the oceans, atmosphere, and climate. Acc. Chem. Res., 50 (3), 599–604.
Colbourn, G., Ridgwell, A., Lenton, T., 2015. The time scale of the silicate weathering negative feedback on atmospheric CO2. Global Biogeochem. Cycles 29, 583–596.
Costa, A.C.G., Marques, F.O., Hildenbrand, A., Sibrant, A.L.R., Catita, C.M.S., 2014. Large-scale catastrophic flank collapses in a steep volcanic ridge: the Pico–Faial Ridge, Azores Triple Junction. J. Volcanol. Geotherm. Res., 272, 111–125.
Costa, A.C.G., Hildenbrand, A., Marques, F.O., Sibrant, A.L.R., de Campos, A.S., 2015. Catastrophic flank collapses and slumping in Pico Island during the last 130 kyr (Pico-Faial ridge, Azores Triple Junction). J. Volcanol. Geotherm. Res., 302, 33–46.
Cresswell-Clay, N., Ummenhofer, C.C., Thatcher, D.L., Wanamaker, A.D., Denniston, R. F., Asmerom, Y., Polyak, V.J., 2022. Twentieth-century Azores High expansion unprecedented in the past 1,200 years. Nat. Geosci., 15 (7), 548–553.
Cruz, J.V., Soares, N., 2018. Groundwater governance in the Azores Archipelago (Portugal): Valuing and protecting a strategic resource in small islands. Water 10 (4), 408.
Delmelle, P., Villiéras, F., Pelletier, M., 2005. Surface area, porosity and water adsorption properties of fine volcanic ash particles. Bull. Volcanol., 67, 160–169.
Dequincey, O., Chabaux, F., Clauer, N., Sigmarsson, O., Liewig, N., Leprun, J.C., 2002. Chemical mobilizations in laterites: evidence from trace elements and 238U-234U-230Th disequilibria. Geochim. Cosmochim. Acta 66 (7), 1197–1210.
Dessert, C., Dupré, B., Gaillardet, J., François, L.M., Allègre, C.J., 2003. Basalt weathering laws and the impact of basalt weathering on the global carbon cycle. Chem. Geol., 202 (3–4), 257–273.
Dessert, C., Lajeunesse, E., Lloret, E., Clergue, C., Crispi, O., Gorge, C., Quidelleur, X., 2015. Controls on chemical weathering on a mountainous volcanic tropical island: Guadeloupe (French West Indies). Geochim. Cosmochim. Acta 171, 216–237.
Dietzen, C., Rosing, M.T., 2023. Quantification of CO2 uptake by enhanced weathering of silicate minerals applied to acidic soils. Int. J. Greenh. Gas Control 125, 103872.
Dixon, J.L., von Blanckenburg, F., 2012. Soils as pacemakers and limiters of global silicate weathering. C. r. Geosci., 344 (11–12), 597–609.
Dosseto, A., Bourdon, B., Turner, S.P., 2008. Uranium-series isotopes in river materials: Insights into the timescales of erosion and sediment transport. Earth Planet. Sci. Lett., 265 (1–2), 1–17.
Dosseto, A., Hannan-Joyner, A., Raines, E., Gayer, E., Michon, L., 2022. Geochemical evolution of soils on Reunion Island. Geochim. Cosmochim. Acta 318, 263–278.
Drever, J.I., Stillings, L.L., 1997. The role of organic acids in mineral weathering. Colloids Surf. a: Physicochem. Eng. Asp., 120 (1–3), 167–181.
Du, X., Rate, A.W., Gee, M.M., 2012. Redistribution and mobilization of titanium, zirconium and thorium in an intensely weathered lateritic profile in Western Australia. Chem. Geol., 330, 101–115.
Dzombak, R.M., Sheldon, N.D., 2020. Weathering intensity and presence of vegetation are key controls on soil phosphorus concentrations: Implications for past and future terrestrial ecosystems. Soil Syst., 4 (4), 73.
Ébelmen, J.J., 1845. Sur les produits de la décomposition des espèces minérales de la famille des silicates. In Annales Des Mines 7, 3–66.
Egli, M., Dahms, D., Norton, K., 2014. Soil formation rates on silicate parent material in alpine environments: Different approaches–different results? Geoderma 213, 320–333.
Emberson, R., Hovius, N., Galy, A., Marc, O., 2016. Chemical weathering in active mountain belts controlled by stochastic bedrock landsliding. Nat. Geosci., 9 (1), 42–45.
Engel, J.M., Ma, L., Sak, P.B., Gaillardet, J., Ren, M., Engle, M.A., Brantley, S.L., 2016. Quantifying chemical weathering rates along a precipitation gradient on Basse-Terre Island, French Guadeloupe: New insight from U-series isotopes in weathering rinds. Geochim. Cosmochim. Acta 195, 29–67.
Frazão, H.C., Prien, R.D., Schulz-Bull, D.E., Seidov, D., Waniek, J.J., 2022. The forgotten Azores current: A long-term perspective. Front. Mar. Sci., 9, 842251.
Gabet, E.J., Mudd, S.M., 2009. A theoretical model coupling chemical weathering rates with denudation rates. Geology 37, 151–154.
Gallagher, T.M., Sheldon, N.D., 2013. A new paleothermometer for forest paleosols and its implications for Cenozoic climate. Geol., 41 (6), 647–650.
Gaillardet, J., Dupré, B., Louvat, P., Allègre, C.J., 1999. Global silicate weathering and CO2 consumption rates deduced from the chemistry of large rivers. Chem. Geol., 159 (1–4), 3–30.
Gaillardet, J., Louvat, P., Lajeunesse, E., 2011a. Rivers from volcanic island arcs: the subduction weathering factory. Appl. Geochem., 26, S350–S353.
Gaillardet, J., Rad, S., Rivé, K., Louvat, P., Gorge, C., Allègre, C.J., Lajeunesse, E., 2011b. Orography-driven chemical denudation in the Lesser Antilles: Evidence for a new feed-back mechanism stabilizing atmospheric CO2. Am. J. Sci., 311 (10), 851–894.
Gillot, P., Cornette, Y., 1986. The Cassignol technique for potassium—Argon dating, precision and accuracy: Examples from the Late Pleistocene to Recent volcanics from southern Italy. Chem. Geol.: Isot Geosci. Sect., 59, 205–222.
Gillot, P., Albore-Livadie, C., Lefèvre, J., Hildebrand, A., 2006. The K/Ar dating method: principle, analytical techniques, and application to Holocene volcanic eruptions in southern Italy. The K/ar Dating Method 1000–1011.
Hasenmueller, E.A., Gu, X., Weitzman, J.N., Adams, T.S., Stinchcomb, G.E., Eissenstat, D. M., Drohan, P., Brantley, S., Kaye, J.P., 2017. Weathering of rock to regolith: The activity of deep roots in bedrock fractures. Geoderma 300, 11–31.
Hernandez, A., Kutiel, H., Trigo, R., Valente, M., Sigró, J., Cropper, T., Santo, E., 2016. New Azores archipelago daily precipitation dataset and its links with large-scale modes of climate variability. Int. J. Climatol., 36 (14), 4439–4454.
Hevia-Cruz, F., Hildenbrand, A., Sheldon, N.D., 2023. Climatic and landscape evolution of the Azores over the past million years: 2020-2023 geochemical and geochronological data. Mendeley Data v1.
Hevia-Cruz, F., Hildenbrand, A., Sheldon, N.D., Hren, M.T., Zanon, V., Marques, F.O., Carlut, J., Chabaux, F., Haurine, F., 2024a. Weathering pulses during glacial-interglacial transitions: insights from well-dated paleosols in the Azores volcanic province (Central North Atlantic). Quat. Sci. Rev., 324, 108438.
Hevia-Cruz, F., Sheldon, N.D., Hildenbrand, A., Hren, M.T., Marques, F.O., Carlut, J., Chabaux, F., 2024b. Regional variations of the Azores High across glacial-interglacial timescales. Paleoceanogr. Paleoclimatol., 39 (5), e2023PA004810.
Hildenbrand, A., Marlin, C., Conroy, A., Gillot, P.Y., Filly, A., Massault, M., 2005. Isotopic approach of rainfall and groundwater circulation in the volcanic structure of Tahiti-Nui (French Polynesia). J. Hydrology 302, 187–208.
Hildenbrand, A., Madureira, P., Marques, F.O., Cruz, I., Henry, B., Silva, P., 2008. Multi-stage evolution of a sub-aerial volcanic ridge over the last 1.3 Myr: S. Jorge Island, Azores Triple Junction. Earth Planet. Sci. Lett., 273 (3–4), 289–298.
Hildenbrand, A., Marques, F.O., Costa, A.C.G., Sibrant, A.L.R., Silva, P.F., Henry, B., Mirande, J.M., Madureira, P., 2012. Reconstructing the architectural evolution of volcanic islands from combined K/Ar, morphologic, tectonic, and magnetic data: The Faial Island example (Azores). J. Volcanol. Geotherm. Res., 241, 39–48.
Hildenbrand, A., Weis, D., Madureira, P., Marques, F.O., 2014. Recent plate re-organization at the Azores Triple Junction: evidence from combined geochemical and geochronological data on Faial, S. Jorge and Terceira Volcanic Islands. Lithos 210, 27–39.
Hildenbrand, A., Marques, F.O., Catalão, J., 2018. Large-scale mass wasting on small volcanic islands revealed by the study of Flores Island (Azores). Sci. Rep., 8 (1), 13898.
Hildenbrand, A., Marques, F.O., Pereira, A., Nomade, S., Hevia-Cruz, F., 2024. Precise dating of large flank collapses by single-grain $^{40}Ar/^{39}Ar$ on pyroclastic deposits from the example of Flores Island (Azores). Sci. Rep., 14, 11905.
Jagoutz, O., Macdonald, F.A., Royden, L., 2016. Low-latitude arc–continent collision as a driver for global cooling. Proc. Natl. Acad. Sci., 113 (18), 4935–4940.
Jobbágy, E.G., Jackson, R.B., 2001. The distribution of soil nutrients with depth: Global patterns and the imprint of plants. Biogeochemistry 53, 51–77.
Johansson, L., Zahirovic, S., Müller, R.D., 2018. The interplay between the eruption and weathering of large igneous provinces and the deep-time carbon cycle. Geophys. Res. Lett., 45 (11), 5380–5389.
Kurtz, A.C., Derry, L.A., Chadwick, O.A., 2001. Accretion of Asian dust to Hawaiian soils: isotopic, elemental, and mineral mass balances. Geochim. Cosmochim. Acta 65 (12), 1971–1983.
Louvat, P., Allègre, C.J., 1997. Present denudation rates on the island of Reunion determined by river geochemistry: basalt weathering and mass budget between chemical and mechanical erosions. Geochim. Cosmochim. Acta 61 (17), 3645–3669.
Louvat, P., Allègre, C.J., 1998. Riverine erosion rates on Sao Miguel volcanic island, Azores Archipelago. Chem. Geol., 148 (3–4), 177–200.
Li, G., Hartmann, J., Derry, L.A., West, A.J., You, C.F., Long, X., Zhan, T., Li, L., Li, G., Qiu, W., 2016. Temperature dependence of basalt weathering. Earth Planet. Sci. Lett., 443, 59–69.
Ma, L., Chabaux, F., Pelt, E., Blaes, E., Jin, L., Brantley, S., 2010. Regolith production rates calculated with uranium-series isotopes at Susquehanna/Shale Hills Critical Zone Observatory. Earth Planet. Sci. Lett., 297 (1–2), 211–225.
Ma, L., Chabaux, F., West, N., Kirby, E., Jin, L., Brantley, S., 2013. Regolith production and transport in the Susquehanna Shale Hills Critical Zone Observatory, part 1: insights from U-series isotopes. J. Geophys. Res. Earth Surf., 118 (2), 722–740.
Marques, F.O., Hildenbrand, A., Hübscher, C., 2018. Evolution of a volcanic island on the shoulder of an oceanic rift and geodynamic implications: S. Jorge Island on the Terceira Rift, Azores Triple Junction. Tectonophys 738, 41–50.
Martin-Garcia, G.M., 2019. Oceanic impact on European climate changes during the Quaternary. Geosci., 9 (3), 119.
Mathieu, D., Bernat, M., Nahon, D., 1995. Short-lived U and Th isotope distribution in a tropical laterite derived from granite (Pitinga river basin, Amazonia, Brazil): application to assessment of weathering rate. Earth Planet. Sci. Lett., 136 (3–4), 703–714.
Meteo France, 2022. Pluviométrie et températures à la Réunion, 14/02/2022. https://meteofrance.re/fr/climat/pluviometrie-et-temperatures-la-reunion (accessed 23 October 2024).
Moore, J.G., 2001. Density of basalt core from Hilo drill hole, Hawaii. J. Volcanol. Geotherm. Res., 112 (1–4), 221–230.
Navarre-Sitchler, A., Brantley, S., 2007. Basalt weathering across scales. Earth Planet. Sci. Lett., 261 (1–2), 321–334.
Nesbitt, H.W., Wilson, R.E., 1992. Recent chemical weathering of basalts. Am. J. Sci., 292 (10), 740–777.
Papelis, C., Wooyong, U., Russell, C.R., Chapman, J.B., 2003. Measuring the specific surface area of natural and man-made glasses: effects of formation process, morphology, and particle size. Colloids Surf A 215, 221–239.

Pelt, E., Chabaux, F., Innocent, C., Navarre-Sitchler, A.K., Sak, P.B., Brantley, S.L., 2008. Uranium–thorium chronometry of weathering rinds: rock alteration rate and paleo-isotopic record of weathering fluids. Earth Planet. Sci. Lett., 276 (1–2), 98–105.
Perez-Fodich, A., Derry, L.A., Marçais, J., Walter, M.T., 2024. The effect of weathering in runoff-to-groundwater partitioning in the Island of Hawai'i: Perspectives for landscape evolution. Earth Planet. Sci. Lett., 635, 118687.
Polacci, M., Pioli, L., Rosi, M., 2003. The Plinian phase of the Campanian Ignimbrite eruption (Phlegrean Fields, Italy): evidence from density measurements and textural characterization of pumice. Bull. Volcanol., 65, 418–432.
Rad, S.D., Allègre, C.J., Louvat, P., 2007. Hidden erosion on volcanic islands. Earth Planet. Sci. Lett., 262 (1–2), 109–124.
Rad, S., Cerdan, O., Rivé, K., Grandjean, G., 2011. Age of river basins in Guadeloupe impacting chemical weathering rates and land use. Appl. Geochem., 26, S123–S126.
Rad, S., Rivé, K., Vittecoq, B., Cerdan, O., Allègre, C.J., 2013. Chemical weathering and erosion rates in the Lesser Antilles: an overview in Guadeloupe, Martinique and Dominica. J. s. Am. Earth Sci., 45, 331–344.
Ritchie, H., Roser, M. 2020. CO_2 emissions. Our World in Data, Oxford Martin School, University of Oxford. https://ourworldindata.org/co2-emissions (accessed 31 May 2024).
Rosi, M., Vezzoli, L., Castelmenzano, A., Grieco, G., 1999. Plinian pumice fall deposit of the Campanian Ignimbrite eruption (Phlegraean Fields, Italy). J. Volcanol. Geotherm. Res., 91 (2–4), 179–198.
Sak, P.B., Murphy, M., Ma, L., Gaillardet, J., Herndon, E.M., Brantley, S.L., Daniel, C., 2018. From unweathered core to regolith in a single weathering andesitic clast: Rates and trends of in situ chemical weathering on a tropical volcanic island (Basse Terre Island, French Guadeloupe). Chem. Geol., 498, 17–30.
Schnoor, J.L., 1990. Kinetics of chemical weathering: a comparison of laboratory and field rates. In: Stumm, W. (Ed.), Aquatic Chemical Kinetics. Wiley, New York, pp. 475–504.
Schopka, H.H., Derry, L.A., 2012. Chemical weathering fluxes from volcanic islands and the importance of groundwater: The Hawaiian example. Earth Planet. Sci. Lett., 339, 67–78.
Schwertmann, U.T.R.M., Taylor, R.M., 1989. Iron oxides. In: Dixon, J.B., Weed, S.B. (Eds.), Minerals in Soil Environments, 2nd ed. Soil Science Society America, Madison.
Sheldon, N.D., 2003. Pedogenesis and geochemical alteration of the Picture Gorge Subgroup, Columbia River Basalt. Oregon. Geol. Soc. Am. Bull., 115, 1377–1387.
Sheldon, N.D., 2006. Using paleosols of the Picture Gorge Basalt to reconstruct the middle Miocene climatic optimum. PaleoBios 26 (2), 27–36.
Sheldon, N.D., Retallack, G.J., 2001. Equation for compaction of paleosols due to burial. Geol., 29 (3), 247–250.
Sheldon, N.D., Tabor, N., 2009. Quantitative paleoenvironmental and paleoclimatic reconstruction using paleosols. Earth-Sci. Rev., 95 (1–2), 1–52.
Sibrant, A., Hildenbrand, A., Marques, F., Weiss, B., Boulesteix, T., Hübscher, C., Lüdmann, T., Costa, A., Catalão, J., 2015. Morpho-structural evolution of a volcanic island developed inside an active oceanic rift: S. Miguel Island (Terceira Rift, Azores). J. Volcanol. Geotherm. Res., 301, 90–106.
Sowards, K.F., Nelson, S.T., McBride, J.H., Bickmore, B.R., Heizler, M.T., Tingey, D.D., Rey, K.A., Yaede, J.R., 2018. A conceptual model for the rapid weathering of tropical ocean islands: A synthesis of geochemistry and geophysics, Kohala Peninsula, Hawaii, USA. Geosphere 14 (3), 1324–1342.
Suresh, P.O., Dosseto, A., Hesse, P.P., Handley, H.K., 2013. Soil formation rates determined from Uranium-series isotope disequilibria in soil profiles from the southeastern Australian highlands. Earth Planet. Sci. Lett., 379, 26–37.
Tabor, N.J., Myers, T.S., 2015. Paleosols as indicators of paleoenvironment and paleoclimate. Ann. Rev. Earth Planet. Sci., 43 (1), 333–361.
von Blanckenburg, F., Schuessler, J., Bouchez, J., Frings, P., Uhlig, D., Oelze, M., Frick, D.A., Hewawasam, T., Dixon, J., Norton, K., 2021. Rock weathering and nutrient cycling along an erodosequence. Am. J. Sci., 321, 1111–1163.
West, A.J., 2012. Thickness of the chemical weathering zone and implications for erosional and climatic drivers of weathering and for carbon-cycle feedbacks. Geology 40 (9), 811–814.
White, A.F., Brantley, S.L., 2003. The effect of time on the weathering of silicate minerals: why do weathering rates differ in the laboratory and field? Chem. Geol., 202 (3–4), 479–506.
White, A.F., Blum, A.E., Schulz, M.S., Bullen, T.D., Harden, J.W., Peterson, M.L., 1996. Chemical weathering of a soil chronosequence on granitic alluvium: 1. Reaction rates based on changes in soil mineralogy. Geochim. Cosmochim. Acta 60, 2533–2550.
Zehetner, F., Gerzabek, M.H., Shellnutt, J.G., Ottner, F., Lüthgens, C., Miggins, D.P., Chen, P.H., Candra, I.N., Schmidt, G., Rechberger, M.V., Sprafke, T., 2020. Linking rock age and soil cover across four islands on the Galápagos archipelago. J. s. Am. Earth Sci., 99, 102500.
Zehetner, F., Gerzabek, M.H., Shellnutt, J.G., Chen, P.H., Candra, I.N., Huang, K.F., Lee, D.C., 2024. Chemical weathering along a one-million-year soil age gradient on the Galápagos Islands. Geochim. Cosmochim. Acta 371, 95–110.